Current Biology 23, 1825–1833, September 23, 2013 ©2013 Elsevier Ltd All rights reserved http://dx.doi.org/10.1016/j.cub.2013.07.054

Report

Talin Autoinhibition Is Required for Morphogenesis

Stephanie J. Ellis,[1] Benjamin T. Goult,[2] Michael J. Fairchild,[1] Nathan J. Harris,[3] Jenny Long,[4] Paolo Lobo,[5] Stefan Czerniecki,[1] Filip Van Petegem,[5] Frieder Schöck,[4] Mark Peifer,[3] and Guy Tanentzapf[1,*]

[1]Department of Cellular and Physiological Sciences, 2350 Health Sciences Mall, University of British Columbia, Vancouver, BC V6T 1Z3, Canada

[2]Department of Biochemistry, University of Leicester, Henry Wellcome Building, Lancaster Road, Leicester LE1 9HN, UK

[3]Department of Biology, University of North Carolina at Chapel Hill, Chapel Hill, NC 27599, USA

[4]Department of Biology, McGill University, 1205 Dr. Penfield Avenue, Montreal, QC H3A 1B1, Canada

[5]Department of Biochemistry and Molecular Biology, 2350 Health Sciences Mall, University of British Columbia, Vancouver, BC V6T 1Z3, Canada

Summary

The establishment of a multicellular body plan requires coordinating changes in cell adhesion and the cytoskeleton to ensure proper cell shape and position within a tissue. Cell adhesion to the extracellular matrix (ECM) via integrins plays diverse, essential roles during animal embryogenesis and therefore must be precisely regulated [1]. Talin, a FERM-domain containing protein, forms a direct link between integrin adhesion receptors and the actin cytoskeleton and is an important regulator of integrin function [2]. Similar to other FERM proteins, talin makes an intramolecular interaction that could autoinhibit its activity [3–6]. However, the functional consequence of such an interaction has not been previously explored in vivo. Here, we demonstrate that targeted disruption of talin autoinhibition gives rise to morphogenetic defects during fly development and specifically that dorsal closure (DC), a process that resembles wound healing, is delayed. Impairment of autoinhibition leads to reduced talin turnover at and increased talin and integrin recruitment to sites of integrin-ECM attachment. Finally, we present evidence that talin autoinhibition is regulated by Rap1-dependent signaling. Based on our data, we propose that talin autoinhibition provides a switch for modulating adhesion turnover and adhesion stability that is essential for morphogenesis.

Results and Discussion

Integrins connect to the cytoskeleton through an intracellular adhesion complex (IAC); changes to the protein composition and interactions within the IAC have important implications for integrin-dependent cellular behaviors [1, 7–9]. Talin is an essential IAC component [2, 10] containing a conserved, integrin-binding 4.1/ezrin/radixin/moesin (FERM) domain at its N terminus and an actin-binding domain at the C terminus of its helical rod domain [2]. Structural studies identified residues in both the talin FERM and rod domains that mediate autoinhibition (Figure 1A) [4, 5]. The same region of the talin FERM domain that binds integrin also binds the rod to mediate autoinhibition [5]. It has been proposed that talin autoinhibition may provide a mechanism to downregulate talin-dependent integrin activation and that blocking talin autoinhibition leads to integrin activation [4, 5]. The biological role of talin autoinhibition is currently not well defined, but initial results in cell culture suggest that it plays an important role as expression of autoinhibition-impaired talin results in increased integrin activation and altered cell spreading [4, 11].

We hypothesized that the mechanism of autoinhibition is conserved between flies and vertebrates. The autoinhibitory regions have been mapped to the F3 lobe of the FERM domain (residues 309–400 in Human Talin1; residues 318–409 in *Drosophila* Talin) and a region of the rod called R9, which forms an amphipathic helical bundle (residues 1655–1826 in mammals; residues 1662–1831 in fly) [5]. The F3 domain is highly conserved across species, with 85.7% protein sequence similarity and 74.7% identity between human talin1 and fly talin (Figure S1A available online). The protein sequence of R9 is also highly conserved, with 56.3% similarity and 33.5% identity (Figure S1B). We used homology modeling to predict the structure of the rod R9 domain based on the NMR structure of mouse talin and found that the fly structure closely resembles that of mouse (Figures 1B and 1C). Notably, four negatively charged surface residues in the rod that are important for autoinhibitory interactions between the FERM and the rod domains are conserved in sequence and arrangement between flies and humans (Figures 1B and 1C). To quantify differences in secondary structure between the mouse nuclear magnetic resonance (NMR) structure and the predicted fly structure, we calculated the root-mean square deviation (rmsd) of the superposition of the two structures (Figure 1D). We obtained a rmsd of 0.148 Å for 635 aligned atoms, suggesting that the two structures are very similar. Homology modeling of the FERM domain also showed excellent conservation between fly and vertebrate (data not shown). We also used NMR spectroscopy to show that the fly R9 domain adopts a stable globular conformation in vitro, similar to the mouse protein homolog (Figures 1E and 1F). Altogether, our homology modeling and NMR data suggest that the domains of mammalian talin and fly talin involved in autoinhibition are likely to be structurally conserved. Importantly, NMR spectroscopy confirmed an interaction between F2-F3 and R9 of fly talin (Figure 1G). This result further confirms the notion that this interaction, which mediates autoinhibition, is conserved between flies and vertebrates.

We sought to design a fly mutant that would specifically disrupt talin autoinhibition. In the R9 domain, we chose to introduce a mutation that was shown, in vitro, to completely abrogate binding with the FERM domain and thus block autoinhibition [5]. This mutation changes a conserved glutamate residue in R9 (E1777 in fly; E1770 in mammalian talin) to an alanine residue (E1777A). NMR analyses demonstrated that the spectra of the region of talin containing the E1777A strongly resembled the spectra of the wild-type (WT) region indicating that the mutation does not disrupt protein folding (Figure 1F).

*Correspondence: tanentz@mail.ubc.ca

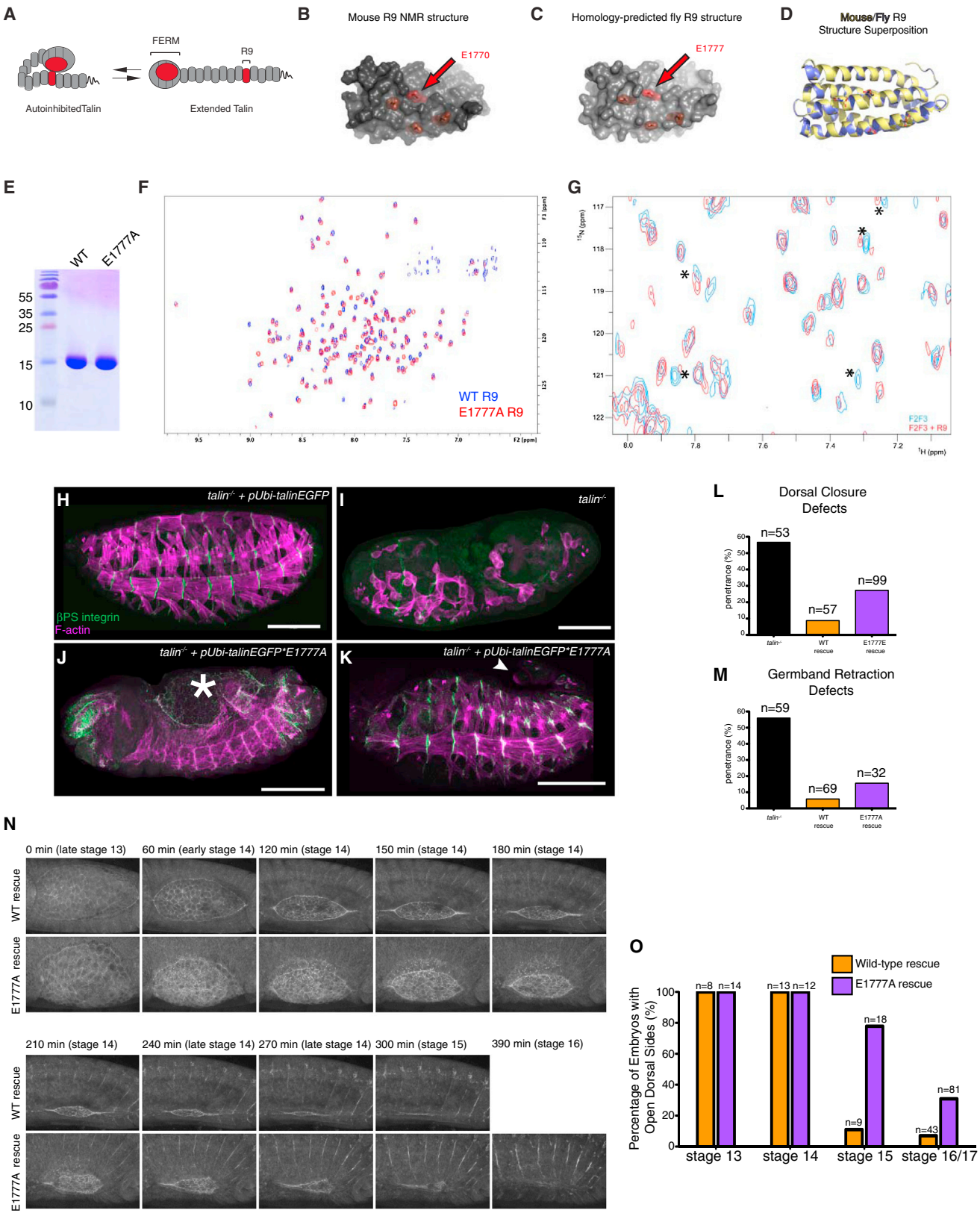

Figure 1. Disruption of a Conserved Autoinhibitory Intramolecular Interaction between the Talin FERM and the Talin Rod Leads to Morphogenetic Defects, Including Delayed Dorsal Closure

(A) Cartoon schematic of talin autoinhibition.
(B–D) The NMR structure [5] of mouse R9 (B) and our homology-predicted model of fly talin R9 (C). Critical residues for F3-rod binding are highlighted in red. Superposition of the mouse NMR structure (yellow) and the homology-modeled fly structure (blue) is shown (D).

(legend continued on next page)

It was not feasible to choose a mutation in the FERM domain to abrogate autoinhibition for two reasons. First, there have only been two mutations in the FERM domain that have been described to disrupt autoinhibition: the role of the first, M319A (equivalent to M328 in flies), is the subject of an unresolved dispute [4, 5, 12]. Second, the other mutation described to disrupt autoinhibition K324D [5] (equivalent to K333D in flies) is adjacent to a residue that is critical for talin function (L325 in vertebrates; L334 in flies) [11, 13, 14]. Moreover, this region of the FERM domain is packed with interaction sites for talin binding partners (Figure S1A). These factors would make it very difficult to interpret, in vivo, the phenotype of mutations in the FERM domain that disrupt talin autoinhibition.

To assess the role of talin autoinhibition, we replaced WT endogenous talin in developing *Drosophila* embryos with rescue transgenes containing the E1777A mutation (see the Supplemental Experimental Procedures). Previous analysis has shown that a ubiquitously expressed WT talin rescue transgene (talinGFP) rescues the embryonic lethality that results when embryos lack both maternal and zygotic talin protein (Figures 1H and 1I) [9]. In comparison, talinGFP*E1777A failed to rescue the lethality associated with loss of talin (Figures 1J and 1K). The ability of talin transgenes to rescue talin mutants was assayed in the context of three different integrin-dependent processes. Two of these, dorsal closure (DC) and germband retraction (GBR), represent dynamic morphogenetic processes, while the third, muscle attachment, represents stable long-term adhesion. While talinGFP fully rescued DC and GBR, talinGFP*E1777A only gave a partial and inconsistent rescue (Figures 1L and 1M). DC occurs late in fly embryogenesis and involves the migration of two epidermal sheets over an extraembryonic epithelium called the amnioserosa (AS); the AS actively contributes to DC [15, 16]. The end result of DC is to create a continuous epidermis on the dorsal side of the embryo. Of embryos rescued with talinGFP*E1777A, 27.3% (n = 99) failed to complete DC, compared with 49.2% (n = 53) of talin-null embryos and 8% (n = 57) of talinGFP-rescued embryos (Figure 1L). However, closer examination of earlier-stage embryos revealed a more penetrant phenotype (Figures 1N and 1O); DC normally concludes at stage 15 in talinGFP-rescued embryos (89% completion rate/stage 15; n = 9) but this was not the case for the majority of talinGFP*E1777A-rescued embryos (22.2% completion rate/stage 15; n = 18). Therefore, talin mutants rescued with talinE1777A exhibited delayed DC (Figure 1O). We confirmed that DC was delayed in talinGFP*E1777A-rescued talin mutants using live time-lapse imaging of rescued embryos (Figure 1N and Movies S1 and S2).

A possible explanation for the delayed and incomplete DC observed in talinGFP*E1777A-rescued embryos is insufficient expression of the mutant talin. Quantitative RT-PCR analysis revealed that transcript levels of talinGFP and the talinGFP*E1777A mutant were approximately equivalent (Figure 2A). Western blot analysis showed that talinGFP*E1777A protein levels were slightly less than those of the talinGFP WT transgene (Figure 2B and 2C). However, the mutant transgenic protein is still present at levels that are comparable to, and even slightly higher than, the levels of endogenous talin protein since the use of the ubiquitin promoter results in slight overexpression of both talinGFP*E1777A and talinGFP relative to endogenous protein (Figures 2B and 2C). Intriguingly, we observe a slight difference in size between talinGFP and talinGFP*E1777A, but we have no evidence to suggest that this has any functional consequence. Importantly, we could not detect a reduction in talin levels via antibody staining at myotendinous junctions (MTJs), suggesting that talinGFP*E1777A transgene expresses sufficiently (Figures S2O and S2P). We also quantified the recruitment of WT talinGFP and talinGFP*E1777A to the prominent integrin adhesions at the MTJs of embryonic muscles using our established protocol [9, 17]. TalinGFP*E1777A was recruited to sites of integrin-mediated adhesion at MTJs better than talinGFP (Figures 2D–2F). This result is reminiscent of recent reports in cultured cells showing that mutating the talin rod to prevent autoinhibition results in increased talin localization in the membrane fraction [12]. Altogether, the defects we observe in talinGFP*E1777A mutant embryos are probably not caused by reduced expression and/or mislocalization of talin but rather by the specific effects of the mutation.

To investigate whether the talinGFP*E1777A impairs the assembly of the IAC and/or its attachment to the extracellular matrix (ECM), we analyzed the fly MTJs as they provide an established and quantitative model to study disruptions in IAC recruitment and ECM attachment [9, 17–19]. We did not find any defects in MTJ integrity, IAC recruitment, or ECM attachment in talin mutant embryos rescued with talinGFP*E1777A (Figures S2A–S2E and S2I–S2O). Previous studies suggested that the ability of talin to autoinhibit might comprise a mechanism to modulate vinculin recruitment and actin association. However, we were unable to find any differences in either actin or vinculin recruitment (Figures S2D, S2E, and S2I–S2L). Additionally, vinculin was not expressed in the AS, providing further evidence that a disruption in vinculin binding to talin was unlikely to underlie the DC defects that we observed in the talinGFP*E1777A-rescued embryos (Figure S2F). We also used gel filtration to confirm that the R9 of the rod domain does not bind vinculin in vitro (Figures S1G and S1H).

Defective morphogenesis could result from improper regulation of stability and turnover of integrin-mediated adhesions. To test this, we studied the adhesion dynamics exhibited by the autoinhibition-defective talinGFP*E1777A using

(E) Coomassie-stained SDS-PAGE gel showing that purified recombinant WT and E1777A fly R9 domains exhibit similar electrophoretic mobility at the expected molecular weight.
(F) $^{1}H,^{15}N$-TROSY-HSQC spectra of 150 μM ^{15}N-labeled WT talin R9 (blue) and R9 E1777A (red). The R9 E1777A mutant shows a well dispersed NMR spectrum similar to that of the wild-type R9, indicating that the mutation does not affect the tertiary structure of the domain.
(G) A $^{1}H,^{15}N$-TROSY-HSQC spectra of 25 μM ^{15}N-labeled fly talin F2F3 alone (blue) or in the presence of the talin rod R9 domain (red). In the presence of R9, some of the peaks have shifted and broadened (indicated by asterisks) compared to the spectra of the free F2F3 providing evidence of a direct interaction between fly F2F3 and R9.
(H–M) Late-stage talin-null embryos stained for integrin (green in H–K) and F-actin (magenta in H–K) were scored for phenotypes in the morphogenetic processes DC (J and L; the asterisk in J demarcates open dorsal hole) and GBR (K and M; the arrowhead in K shows the unretracted tail). Embryos were rescued with talinGFP (H) construct or the talinGFP*E1777A autoinhibition mutant construct (J and K).
(N and O) Talin-null embryos rescued with either talinGFP or talinGFP*E1777A were scored for dorsal holes at stage 13–17 (O; see the Supplemental Experimental Procedures). Images from time-lapse movies of WT-rescued embryos (top) or E1777A mutant (bottom) embryos expressing talinGFP*E1777A and undergoing DC at the indicated time-points are shown (N).
Scale bars represent 100 μm. See also Figures S1 and S2 and Movies S1 and S2.

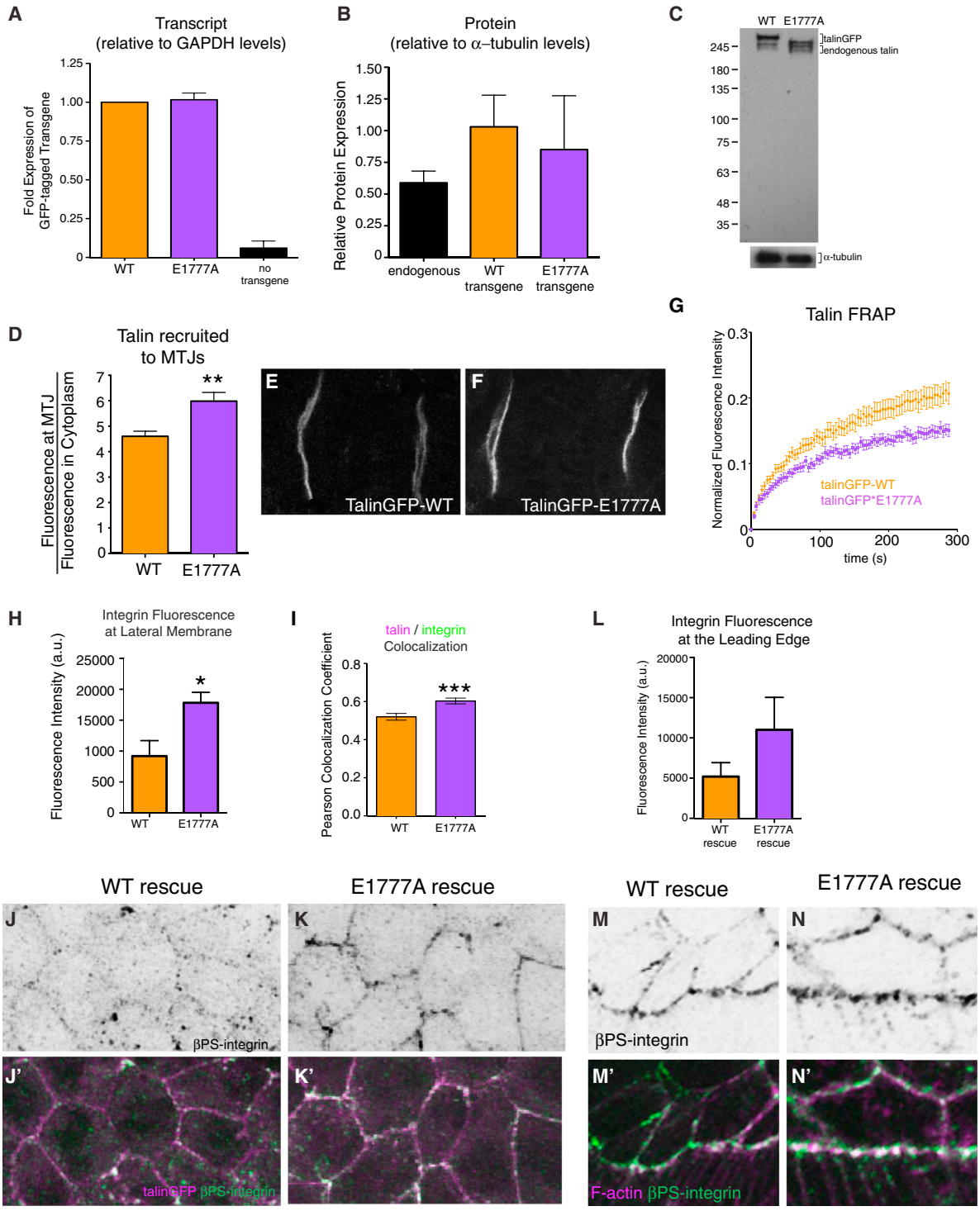

Figure 2. Talin Recruitment and Adhesion Dynamics Are Altered by the E1777A Autoinhibition Mutation

(A–C) Quantitative PCR (A) and western blot (B and C) data for talinGFP (orange), autoinhibition mutant talinGFP*E1777A (purple), and endogenous untagged talin (black). Talin was detected with a polyclonal antibody raised to the C terminus (see [10]), and western blots were done in a wild-type background.

(D–F) The recruitment of talinGFP (D and E) and talinGFP*E1777A (D and F) at MTJs (D, **$p < 0.01$).

(G) Fluorescence recovery curves of talinGFP (orange) and talinGFP*E1777A (purple) obtained from FRAP experiments on embryonic MTJs.

(H–N) βPS-integrin signal was quantified at the lateral membrane of AS cells (H) and the leading edge of the epidermis (L) and colocalization of talin (magenta in J′ and K′) and βPS integrin (green in J′–K′ and M′–N′; black in J–K and M–N) was measured at the lateral membrane of AS cells using Pearson correlation coefficients (I; $n > 25$ cells, *$p < 0.05$, ***$p < 0.001$). F-actin is shown in magenta in (M′)–(N′) to highlight the leading edge.

Error bars indicate the SEM. Scale bars represent 10 μm.

our previously established fluorescence recovery after photobleaching (FRAP) protocol to examine the turnover of integrin and IAC components at MTJs in living *Drosophila* embryos and larvae [18]. FRAP analysis revealed that talinGFP*E1777A is more stable at MTJs than is WT talinGFP (Figure 2G). These data suggest that talin autoinhibition can modulate the turnover of integrin-based adhesion and that, specifically, prevention of talin autoinhibition stabilizes the adhesion complex. Further examination of integrin-mediated adhesions in the AS supported this idea. We found that embryos rescued with talinGFP*E1777A exhibited greater integrin recruitment to the membrane of AS cells (Figures 2H, 2J′, and 2K′) and also to the leading edge of the epidermal cells that crawl over the AS (Figures 2L–2N). We also observed increased colocalization of talin and integrin in the AS (Figures 2I–2K). These observations are in line with reports in culture that expression of the talin*E1770A autoinhibition mutant resulted in increased focal adhesion assembly [11].

Our results indicated a link between autoinhibition and the regulation of the turnover and stability of integrin-based adhesions. The signaling molecules focal adhesion kinase (FAK) and Rap1 have been implicated in such regulation [20–22], and we sought to see whether either effector acts to regulate talin autoinhibition. Analysis of FAK failed to show any phenotypic parallels or genetic interactions with disrupted talin autoinhibition; loss of FAK does not lead to defects in embryogenesis or disrupt viability [23]. Moreover, modulation of FAK activity does not impinge on turnover of either WT talinGFP or the talinGFP*E1777A at MTJs (Figure S3). We also tested the small GTPase Rap1, which has been implicated as part of a putative complex that localizes talin from the cytoplasm to adhesion complexes at the plasma membrane [24, 25], where it has been speculated autoinhibition can be relieved [14, 26, 27]. Our hypothesis was that increasing Rap1 activity would give rise to similar phenotypes to those observed in talinGFP*E1777A-rescued embryos. To test this, we expressed a constitutively-active form of Rap1 (Rap1-Q63E; Rap1-CA) in the AS using the tissue-specific Gal4 driver c381; we observed similar DC defects to those seen with the autoinhibition-defective talin (Figure 3). Specifically, more than 60% of the Rap1-CA-expressing embryos had open dorsal holes at the end of stage 15 with about 20% of the embryos failing to complete DC altogether (Figures 3A and 3B). We confirmed this delay using time-lapse imaging (Figure 3A and Movies S3 and S4). Furthermore, we found that colocalization of integrin and talin was increased in integrin-mediated adhesions of AS cells expressing Rap1-CA—this manifested itself as an increase in integrin signal at the membrane (Figures 3C–3F). We also tested the effect of expressing a dominant-negative form of Rap1 (Rap1-S17A; Rap1-DN) specifically in the AS and found that it also gave rise to DC defects. However, the Rap1-DN phenotype is different from that observed with the Rap1-CA in two ways: (1) DC was not delayed but rather failed outright and (2) other morphogenetic problems, such as failed GBR, were observed (Figure S4) Our data are consistent with previous work showing that expressing either Rap1-CA or Rap1-DN in the fly epidermis impairs DC, although the severity and range of phenotypes observed was different [28]. Altogether, these results indicate that Rap1 modulates integrin adhesion in the AS and is required for DC.

In addition to regulating integrin recruitment to the membrane in the AS, we also found that Rap1-CA increased the recruitment of talinGFP to MTJs (Figure 3G). Therefore, we predicted that Rap1 might also regulate IAC turnover. FRAP analysis of talinGFP dynamics at MTJs revealed decreased turnover upon expression of Rap1-CA in the muscle (Figure 3I). In comparison, expression of Rap1-DN elicited the opposite effect: turnover of talinGFP increased (Figure 3J). To test whether Rap1 conferred its effect upstream of talin autoinhibition, we expressed either Rap1-DN or Rap1-CA in the presence of the talin autoinhibition mutant, talinGFP*E1777A. We found that Rap1-CA did not affect talinGFP*E1777A recruitment (Figure 3H) and that neither Rap1-CA nor Rap1-DN modulated talinGFP*E1777A turnover (Figures 3K and 3L). These results suggest that active Rap1 increases talin recruitment to and stabilization at cell-ECM adhesions and that this effect occurs upstream of talin autoinibition.

It has been shown that the Mig-10/RIAM/lamellipodin (MRL) family protein Rap1-GTP-interacting adaptor molecule (RIAM) links membrane targeting sequences in Rap1 to talin, thereby recruiting talin to the plasma membrane, leading to activation of integrin and enhanced adhesion [24, 29]. In general, the functions assigned to RIAM, including recruiting talin to the membrane and promoting stable adhesions, are similar to those obtained by the relief of autoinhibition [12, 25, 29, 30]. Comprehensive analyses of the embryonic role of the *Drosophila* RIAM homolog, *pico*, are precluded at this time because the original loss-of-function allele has been lost. To circumvent this problem and to test whether RIAM may also be involved in Rap1-dependent regulation of talin autoinhibition in the fly, we developed alternative approaches to modulate pico/RIAM levels in the embryo. First, we used a minimal RIAM-Rap1 chimera (Figure 4A; "RIAM30-CAAX") comprised of the first 30 amino acids of human RIAM, which contains a talin binding site, and the membrane-targeting CAAX sequence of Rap1a, that was previously shown to be sufficient to activate integrins in CHO cells [24]. We found that expression of RIAM30-CAAX in the AS leads to delays in dorsal closure: approximately 80% of embryos exhibited open dorsal sides at the end of stage 15 (Figures 4B and 4C). Furthermore, we found that RIAM30-CAAX induced increased recruitment of talinGFP to the membrane (Figure 4D) and that the turnover dynamics of talinGFP decreased (Figure 4G). The phenotypes conferred by increasing pico/RIAM via RIAM30-CAAX closely resembled those elicited by both the talinGFP*E1777A mutant and Rap1-CA, suggesting that pico/RIAM could play a similar role in regulation of talin function. The ability of a human protein chimera to work as well as it does in flies illustrates the conservation of this system throughout evolution. Second, using an RNA interference (RNAi)-induced knockdown of *pico* in the muscles, we found that the turnover of talinGFP increased (Figures 4F and 4H), recapitulating the observed effect of expressing Rap1-DN. Importantly, neither the recruitment of talinGFP*E1777A to the membrane (Figure 4E) nor the turnover dynamics of talinGFP*E1777A changed upon modulation of pico/RIAM levels (Figures 4I and 4J), indicating that, like Rap1, pico/RIAM modulates talin behavior via an autoinhibition-dependent mechanism. We propose that Rap1 and RIAM act upstream of talin to relieve autoinhibition; this promotes its recruitment to sites of adhesion, where it forms a stabilizing link between integrins and the cytoskeleton (Figure 4K). Our results also support the notion that a nonautoinhibited talin molecule can be recruited independent of Rap1/RIAM activity.

Overall, this study identifies an important role for the regulation of talin function through autoinhibition. Failure to autoinhibit talin impairs morphogenetic processes, but this is not due to defects in integrin-mediated attachment to the ECM or in the

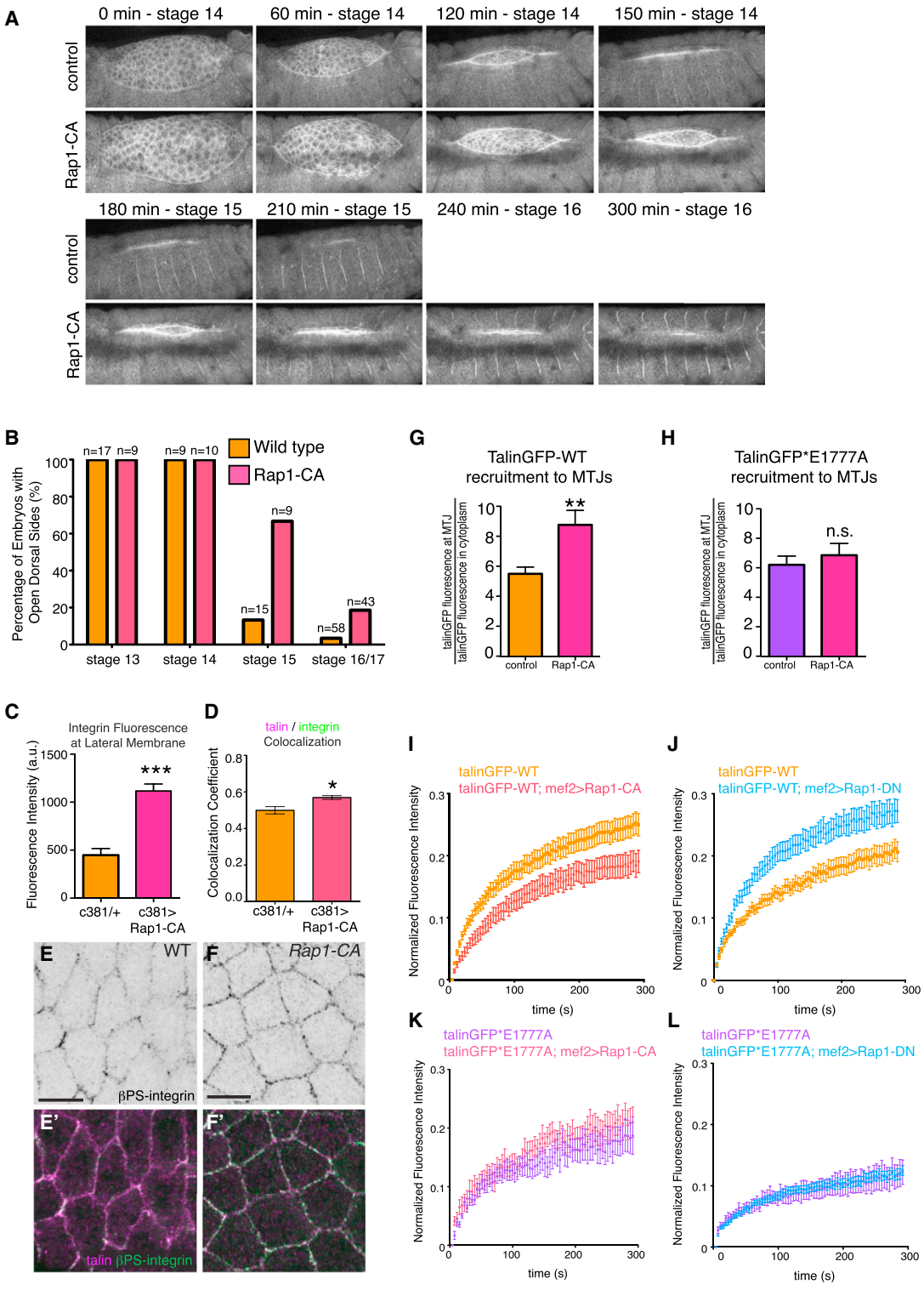

Figure 3. Rap1 Functions Upstream of Talin Autoinhibition during Morphogenesis

(A) WT embryos and embryos expressing Rap1-CA in the AS were scored for openings in the dorsal epidermis at stage 13–17.

(B) Images from time-lapse movies of control embryos (top) or embryos expressing Rap1-CA in the AS (bottom) undergoing DC at the indicated time-points.

(C–F) β-integrin signal localized at the lateral membrane of AS cells was quantified (C), and colocalization of talin (magenta in E′ and F′) and β-integrin (black in E and F; green in E′ and F′) was measured at the membrane of AS cells using Pearson correlation coefficients (D; n > 25 cells, *p < 0.05,***p < 0.001).

(G and H) The recruitment of talinGFP (G) and talinGFP*E1777A (H) to MTJs was measured in control embryos (orange in G; purple in H) and embryos expressing Rap1CA (pink; **p < 0.01).

(I–L) FRAP experiments were performed on talinGFP (I and J) and talinGFP*E1777A (K and L) to determine the effect of expressing either Rap1-CA (I and K) or Rap1-DN (J and L) on the mobility of talin at MTJs.

Error bars indicate the SEM. Scale bars represent 10 μm. See also Figures S3 and S4 and Movies S3 and S4.

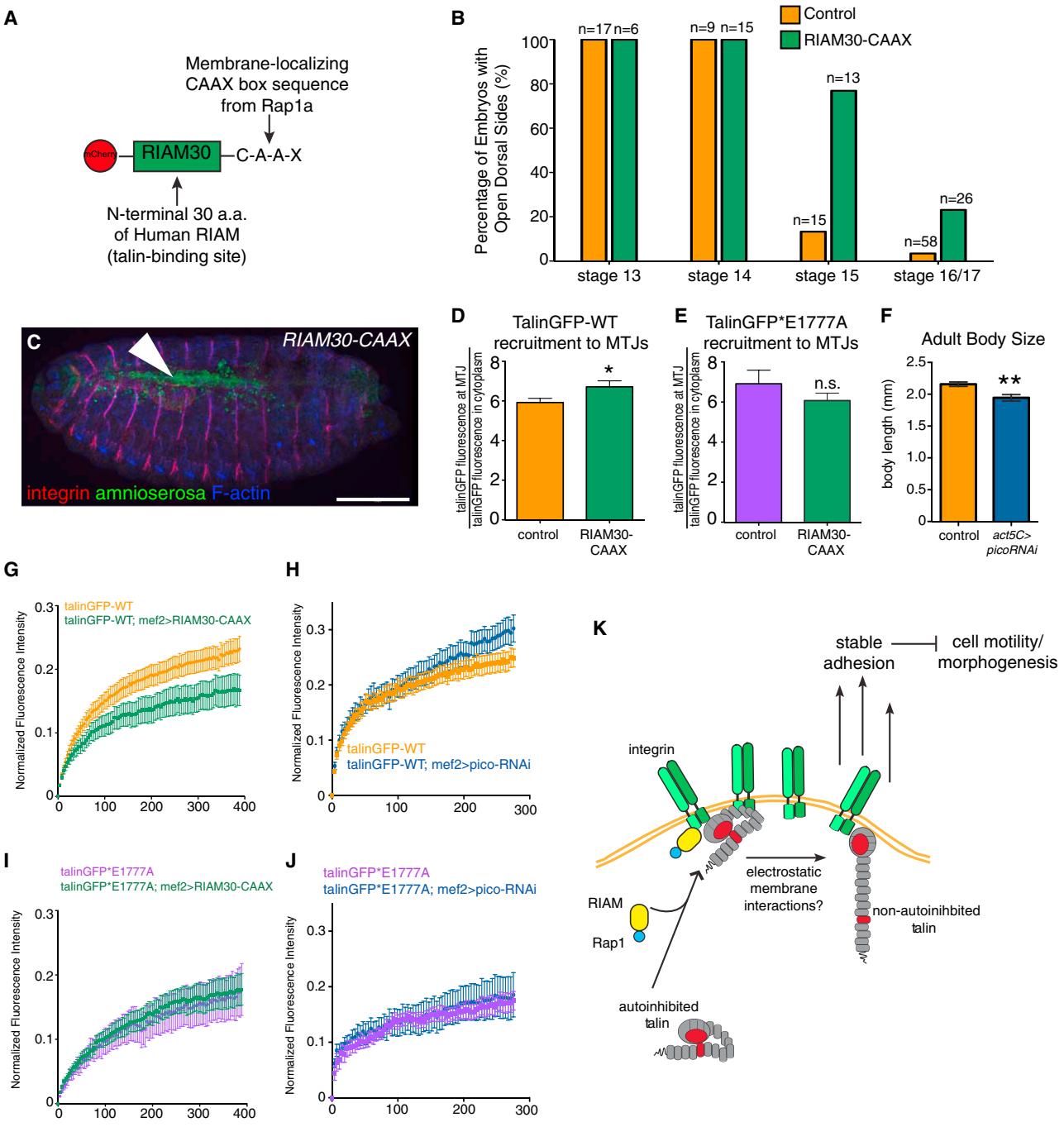

Figure 4. Pico/RIAM Functions Upstream of Talin Autoinhibition during Morphogenesis

(A) Schematic diagram of RIAM30-CAAX.

(B) WT embryos and embryos expressing RIAM30-CAAX in the AS were scored for openings in the dorsal epidermis at stage 13–17.

(C) Stage 15 embryo with an open dorsal hole (arrowhead) stained for amnioserosa (green), integrin (red), and F-actin (blue).

(D and E) The recruitment of talinGFP (D) and talinGFP*E1777A (E) to MTJs in control embryos and embryos expressing RIAM30-CAAX.

(F) To provide evidence of *pico* knockdown based on the previously described *pico* phenotype [31], we measured adult body size of control embryos and embryos expressing picoRNAi under the control of a ubiquitous driver.

(G–J) FRAP experiments were performed on talinGFP (G and H) and talinGFP*E1777A (I and J) to determine the effect of expressing either RIAM30-CAAX (G and I) or picoRNAi (H and J) on the mobility of talin at MTJs.

(K) Model for the role and regulation of talin autoinhibition. RIAM-Rap1 acts to localize autoinhibited talin to integrin-mediated adhesions, where autoinhibition can be relieved by electrostatic membrane interactions. This mechanism promotes stable adhesion, thus downregulating cell motility required for morphogenesis.

Error bars indicate the SEM. Scale bars represent 100 μm.

assembly of the adhesion complex. Thus, it is unlikely that the E1777A mutation blocks integrin-mediated cell-ECM attachment in a dominant-negative fashion. An alternative explanation for the phenotype is that the E1777A mutant behaves like a gain-of-function allele of talin and that the morphogenetic defects that we observe are due to too much rather than too little adhesion. This would not be the first time such a phenomenon has been observed; for example, overexpression of integrins in either the wing or the muscle gives rise to phenotypes identical to those found in integrin-null mutants [17, 32]. How could the E1777A mutation give rise to stronger adhesion? We show that this mutation enhances the recruitment and colocalization of talin and integrin at sites of adhesion. Importantly, we show that the E1777A mutation effectively reduces talin turnover at sites of adhesion. Indeed, our data fit with a gain-of-function model: blocking talin autoinhibition leads to increased integrin-mediated adhesion, and this impairs morphogenetic processes that require cyclic adhesion assembly and disassembly. Further consistent with this model is the observation that adhesion at MTJs, a nonmorphogenetic context, is not perturbed upon blocking autoinhibition of talin. We cannot exclude the possibility that E1777A may confer its effect on talin function through a means other than disruption of autoinhibition. Encouragingly, however, our homology modeling and NMR analyses strongly suggest that the fly protein behaves much as the mammalian homolog does.

How does prevention of autoinhibition stabilize integrin-mediated adhesion? We show that autoinhibition regulates talin recruitment to adhesions through a RIAM-Rap1-dependent mechanism. Interestingly, the E1777A autoinhibition mutant talin is more strongly recruited to adhesions than WT talin; this enhanced recruitment occurs independent of RIAM-Rap1 activity. Thus, it is possible that constitutive relief of autoinhibition works to stabilize and promote adhesion by enhancing recruitment of the talin molecule to adhesions, thus bypassing the need of the RIAM-Rap1 pathway for recruitment. At the membrane, adhesion strengthening may occur via talin's scaffolding function, as talin can interact with multiple components of the IAC, and these interactions may increase and/or change when talin assumes a more extended conformation. Another possibility, consistent with structural studies, is that relief of autoinhibition frees up the FERM/IBS-1 domain of talin such that it can activate integrins [4, 5]. We would predict that mutations in talin that block IBS-1-mediated integrin activation would lead to more dynamic adhesions, and this is indeed what was observed [9]. According to the model we envision, talin recruitment is determined by the sum of interactions that a single molecule can make with other IAC components at any one time. For example, the autoinhibited form of talin relies on Rap1/RIAM for efficient recruitment, even though it may still bind integrin through its free IBS-2 domain [9]; both mechanisms may contribute to targetting of talin to adhesions. We speculate that relief of autoinhibition makes the IBS-1 available, as well as the many other binding sites for IAC components that are found in the talin rod domain (e.g., vinculin binding sites), thereby substantially increasing the number of possible interactions that can lead to talin recruitment to the IAC.

There are likely to be multiple avenues leading to relief of talin autoinhibition. Recent superresolution studies provided elegant evidence that autoinhibition is primarily relieved within adhesion complexes [27], implicating the need for a mechanism to specifically recruit autoinhibited talin to adhesions. Here we show that forcing talin to remain in an open, nonautoinhibited conformation gives rise to very similar phenotypes as activating the RIAM-Rap1 pathway. Based on the results obtained by us and other groups [6, 14, 25, 27, 29, 33, 34], we propose that RIAM-Rap1 brings autoinhibited talin to the membrane where autoinhibition can subsequently be relieved, possibly through electrostatic interactions with the membrane/PIP2. RIAM-Rap1 has a previously established role in mediating the recruitment of talin to sites of adhesion, but it has recently been demonstrated that the requirement for RIAM-Rap1 is context dependent. Structural and biochemical studies have revealed that the binding of talin to either RIAM or vinculin is mutually exclusive and likely dependent on force [32, 34]. Moreover, in cell culture, vinculin-stimulated integrin activation is RIAM-Rap1 independent, raising the possibility that more mature adhesions might not need RIAM-Rap1 to promote talin activation in this case [33]. Along similar lines, we demonstrate that RIAM-Rap1 activity is dispensable for recruitment of a nonautoinhibited talin molecule.

In summary, our results suggest that talin autoinhibition confers a switch through which fine control of integrin-mediated adhesion can be exerted in vivo. Our findings also reveal RIAM-Rap1-mediated regulation of integrin adhesion to be an important modulator of morphogenesis and provide evidence for an autoinhibition-based pathway for control of talin function through RIAM-Rap1. Furthermore, this study exemplifies how subtle tuning of adhesion complex composition and stability elicits different adhesive functions and cellular behaviors during development.

Supplemental Information

Supplemental Information includes Supplemental Experimental Procedures, four figures, and four movies and can be found with this article online at http://dx.doi.org/10.1016/j.cub.2013.07.054.

Acknowledgments

We thank James Lim for the RIAM30-CAAX construct, Lisa Fessler for antibodies, and Nick Harden for fly lines. We thank David Calderwood for helpful discussion and Katie Goodwin for technical assistance. This work was funded through Canadian Institutes of Health Research operating grants MOP-123210 (G.T.) and MOP-93727 (F.S.) and National Institutes of Health grant R01 GM47857 (M.P.). S.J.E. and M.J.F. hold NSERC Alexander Graham Bell Canada Graduate Scholarships. G.T. is a CIHR New Investigator and Michael Smith Foundation for Health Research Scholar.

Received: January 16, 2013
Revised: June 24, 2013
Accepted: July 16, 2013
Published: September 5, 2013

References

1. Bulgakova, N.A., Klapholz, B., and Brown, N.H. (2012). Cell adhesion in Drosophila: versatility of cadherin and integrin complexes during development. Curr. Opin. Cell Biol. *24*, 702–712.
2. Critchley, D.R. (2009). Biochemical and structural properties of the integrin-associated cytoskeletal protein talin. Annu Rev Biophys *38*, 235–254.
3. Tepass, U. (2009). FERM proteins in animal morphogenesis. Curr. Opin. Genet. Dev. *19*, 357–367.
4. Goksoy, E., Ma, Y.Q., Wang, X., Kong, X., Perera, D., Plow, E.F., and Qin, J. (2008). Structural basis for the autoinhibition of talin in regulating integrin activation. Mol. Cell *31*, 124–133.
5. Goult, B.T., Bate, N., Anthis, N.J., Wegener, K.L., Gingras, A.R., Patel, B., Barsukov, I.L., Campbell, I.D., Roberts, G.C., and Critchley, D.R. (2009). The structure of an interdomain complex that regulates talin activity. J. Biol. Chem. *284*, 15097–15106.

6. Song, X., Yang, J., Hirbawi, J., Ye, S., Perera, H.D., Goksoy, E., Dwivedi, P., Plow, E.F., Zhang, R., and Qin, J. (2012). A novel membrane-dependent on/off switch mechanism of talin FERM domain at sites of cell adhesion. Cell Res. *22*, 1533–1545.
7. Askari, J.A., Buckley, P.A., Mould, A.P., and Humphries, M.J. (2009). Linking integrin conformation to function. J. Cell Sci. *122*, 165–170.
8. Geiger, B., and Yamada, K.M. (2011). Molecular architecture and function of matrix adhesions. Cold Spring Harb. Perspect. Biol. *3*, a005033.
9. Ellis, S.J., Pines, M., Fairchild, M.J., and Tanentzapf, G. (2011). In vivo functional analysis reveals specific roles for the integrin-binding sites of talin. J. Cell Sci. *124*, 1844–1856.
10. Brown, N.H., Gregory, S.L., Rickoll, W.L., Fessler, L.I., Prout, M., White, R.A., and Fristrom, J.W. (2002). Talin is essential for integrin function in Drosophila. Dev. Cell *3*, 569–579.
11. Kopp, P.M., Bate, N., Hansen, T.M., Brindle, N.P., Praekelt, U., Debrand, E., Coleman, S., Mazzeo, D., Goult, B.T., Gingras, A.R., et al. (2010). Studies on the morphology and spreading of human endothelial cells define key inter- and intramolecular interactions for talin1. Eur. J. Cell Biol. *89*, 661–673.
12. Banno, A., Goult, B.T., Lee, H., Bate, N., Critchley, D.R., and Ginsberg, M.H. (2012). Subcellular localization of talin is regulated by inter-domain interactions. J. Biol. Chem. *287*, 13799–13812.
13. Wegener, K.L., Partridge, A.W., Han, J., Pickford, A.R., Liddington, R.C., Ginsberg, M.H., and Campbell, I.D. (2007). Structural basis of integrin activation by talin. Cell *128*, 171–182.
14. Saltel, F., Mortier, E., Hytönen, V.P., Jacquier, M.C., Zimmermann, P., Vogel, V., Liu, W., and Wehrle-Haller, B. (2009). New PI(4,5)P2- and membrane proximal integrin-binding motifs in the talin head control beta3-integrin clustering. J. Cell Biol. *187*, 715–731.
15. Frank, L.H., and Rushlow, C. (1996). A group of genes required for maintenance of the amnioserosa tissue in Drosophila. Development *122*, 1343–1352.
16. Solon, J., Kaya-Copur, A., Colombelli, J., and Brunner, D. (2009). Pulsed forces timed by a ratchet-like mechanism drive directed tissue movement during dorsal closure. Cell *137*, 1331–1342.
17. Tanentzapf, G., Martin-Bermudo, M.D., Hicks, M.S., and Brown, N.H. (2006). Multiple factors contribute to integrin-talin interactions in vivo. J. Cell Sci. *119*, 1632–1644.
18. Yuan, L., Fairchild, M.J., Perkins, A.D., and Tanentzapf, G. (2010). Analysis of integrin turnover in fly myotendinous junctions. J. Cell Sci. *123*, 939–946.
19. Tanentzapf, G., and Brown, N.H. (2006). An interaction between integrin and the talin FERM domain mediates integrin activation but not linkage to the cytoskeleton. Nat. Cell Biol. *8*, 601–606.
20. Ren, X.D., Kiosses, W.B., Sieg, D.J., Otey, C.A., Schlaepfer, D.D., and Schwartz, M.A. (2000). Focal adhesion kinase suppresses Rho activity to promote focal adhesion turnover. J. Cell Sci. *113*, 3673–3678.
21. Lawson, C., Lim, S.T., Uryu, S., Chen, X.L., Calderwood, D.A., and Schlaepfer, D.D. (2012). FAK promotes recruitment of talin to nascent adhesions to control cell motility. J. Cell Biol. *196*, 223–232.
22. Freeman, S.A., McLeod, S.J., Dukowski, J., Austin, P., Lee, C.C., Millen-Martin, B., Kubes, P., McCafferty, D.M., Gold, M.R., and Roskelley, C.D. (2010). Preventing the activation or cycling of the Rap1 GTPase alters adhesion and cytoskeletal dynamics and blocks metastatic melanoma cell extravasation into the lungs. Cancer Res. *70*, 4590–4601.
23. Grabbe, C., Zervas, C.G., Hunter, T., Brown, N.H., and Palmer, R.H. (2004). Focal adhesion kinase is not required for integrin function or viability in Drosophila. Development *131*, 5795–5805.
24. Lee, H.S., Lim, C.J., Puzon-McLaughlin, W., Shattil, S.J., and Ginsberg, M.H. (2009). RIAM activates integrins by linking talin to ras GTPase membrane-targeting sequences. J. Biol. Chem. *284*, 5119–5127.
25. Han, J., Lim, C.J., Watanabe, N., Soriani, A., Ratnikov, B., Calderwood, D.A., Puzon-McLaughlin, W., Lafuente, E.M., Boussiotis, V.A., Shattil, S.J., and Ginsberg, M.H. (2006). Reconstructing and deconstructing agonist-induced activation of integrin alphaIIbbeta3. Curr. Biol. *16*, 1796–1806.
26. Martel, V., Racaud-Sultan, C., Dupe, S., Marie, C., Paulhe, F., Galmiche, A., Block, M.R., and Albiges-Rizo, C. (2001). Conformation, localization, and integrin binding of talin depend on its interaction with phosphoinositides. J. Biol. Chem. *276*, 21217–21227.
27. Rossier, O., Octeau, V., Sibarita, J.B., Leduc, C., Tessier, B., Nair, D., Gatterdam, V., Destaing, O., Albigès-Rizo, C., Tampé, R., et al. (2012). Integrins β1 and β3 exhibit distinct dynamic nanoscale organizations inside focal adhesions. Nat. Cell Biol. *14*, 1057–1067.
28. Boettner, B., Harjes, P., Ishimaru, S., Heke, M., Fan, H.Q., Qin, Y., Van Aelst, L., and Gaul, U. (2003). The AF-6 homolog canoe acts as a Rap1 effector during dorsal closure of the Drosophila embryo. Genetics *165*, 159–169.
29. Worth, D.C., Hodivala-Dilke, K., Robinson, S.D., King, S.J., Morton, P.E., Gertler, F.B., Humphries, M.J., and Parsons, M. (2010). Alpha v beta3 integrin spatially regulates VASP and RIAM to control adhesion dynamics and migration. J. Cell Biol. *189*, 369–383.
30. Lafuente, E.M., van Puijenbroek, A.A., Krause, M., Carman, C.V., Freeman, G.J., Berezovskaya, A., Constantine, E., Springer, T.A., Gertler, F.B., and Boussiotis, V.A. (2004). RIAM, an Ena/VASP and Profilin ligand, interacts with Rap1-GTP and mediates Rap1-induced adhesion. Dev. Cell *7*, 585–595.
31. Lyulcheva, E., Taylor, E., Michael, M., Vehlow, A., Tan, S., Fletcher, A., Krause, M., and Bennett, D. (2008). Drosophila pico and its mammalian ortholog lamellipodin activate serum response factor and promote cell proliferation. Dev. Cell *15*, 680–690.
32. Brabant, M.C., Fristrom, D., Bunch, T.A., and Brower, D.L. (1996). Distinct spatial and temporal functions for PS integrins during Drosophila wing morphogenesis. Development *122*, 3307–3317.
33. Lee, H.S., Anekal, P., Lim, C.J., Liu, C.C., and Ginsberg, M.H. (2013). Two modes of integrin activation form a binary molecular switch in adhesion maturation. Mol. Biol. Cell *24*, 1354–1362.
34. Goult, B.T., Zacharchenko, T., Bate, N., Tsang, R., Hey, F., Gingras, A.R., Elliott, P.R., Roberts, G.C., Ballestrem, C., Critchley, D.R., and Barsukov, I.L. (2013). RIAM and vinculin binding to talin are mutually exclusive and regulate adhesion assembly and turnover. J. Biol. Chem. *288*, 8238–8249.

Current Biology, Volume *23*

Supplemental Information

Talin Autoinhibition Is Required for Morphogenesis

Stephanie J. Ellis, Benjamin T. Goult, Michael J. Fairchild, Nathan J. Harris Jenny Long, Paolo Lobo, Stefan Czerniecki, Filip Van Petegem, Frieder Schöck, Mark Peifer, and Guy Tanentzapf

A Alignment of Talin F3 domain (mammalian residues 292-411)

B Alignment of Talin R9 (mammalian 1652 - 1831 residues)

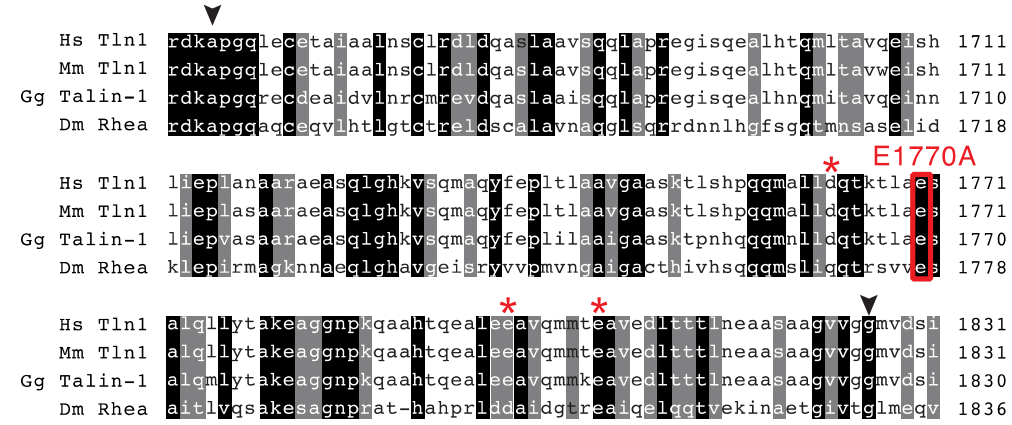

Figure S1. Species alignment of domains required for talin autoinhibition, Related to Figure 1. Alignment of Human (Hs Tln1), Mouse (Mm Tln1), Chicken (Gg Talin-1), and fly (Dm Rhea) talin FERM F3 (A) and R9 (B). Arrowheads bracket the specific, structurally defined regions. Red asterisks: residues implicated in autoinhibition; green asterisks: residues implicated in other F3-dependent interactions.

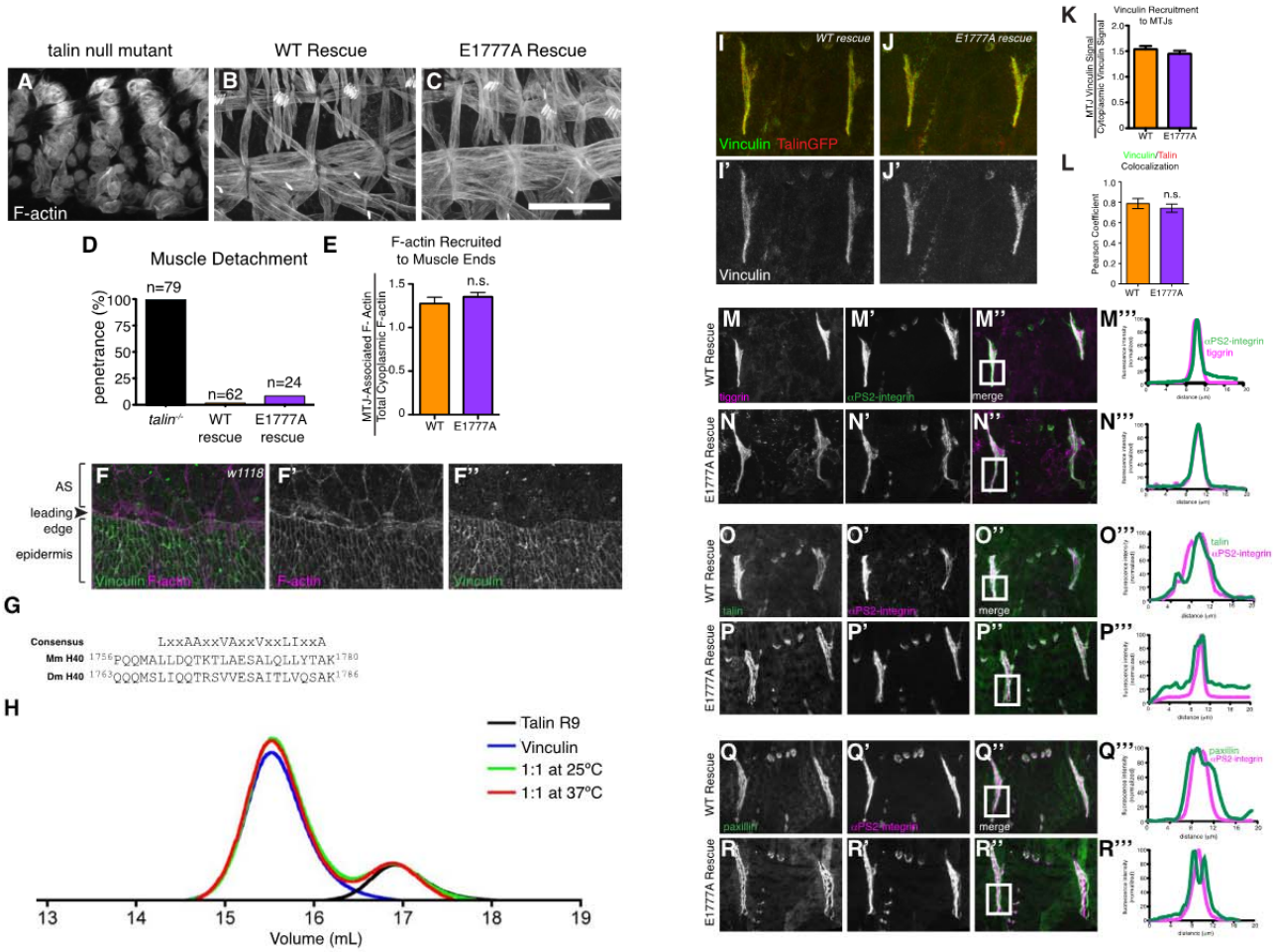

Figure S2. Talin autoinhibition is not required to maintain muscle attachment to the ECM or for IAC assembly at MTJs, Related to Figure 1. (**A-C**) Confocal z-stacks of muscles of talin null embryos (A), WT-rescued embryos (B), and E1777A rescued embryos (C) stained with phalloidin to label F-actin to show muscle morphology. (**D**) Penetrance of muscle attachment defects in stage 17 embryos for each of the indicated genotypes. (**E**) Recruitment of actin to muscle ends in WT-rescued (orange) and E1777A-rescued (purple) talin mutant embryos. (**F**) Stage 14 embryo stained for F-actin (magenta in F; grey in F') and vinculin (green in F; grey in F''). Vinculin is not expressed in the amnioserosa. (**G**) Sequence alignment of Helix 40 of mouse (top) and fly (bottom) talin. The consensus vinculin binding sequence is shown below. (**H**) Analytical gel filtration of R9 mixed with vinculin Vd1 indicating that vinculin and R9 do not bind. (**I-L)** Confocal z-stacks of MTJs in embryos expressing talinGFP (I) or talinGFP*E1777A (J) and stained for vinculin (green in I-J; grey in I'-J') and talinGFP (red in I-J). Vinculin recruitment (K) and colocalization of vinculin and talin (L) were measured at MTJs (**M-R**) Confocal z-stacks of MTJs in talin-null embryos rescued with either talinGFP (M,O,Q) or the talinGFP*E1777A autoinhibtion mutant (N,P,R) labelled for tiggrin (grey in M,N; magenta in M'', N''), α–integrin (grey in M',N',O',P'Q'R'; green in M'',N''; magenta in O',P',Q',R'), talin (grey in O-P, green in O''-P'') and paxillin (grey in Q, R; green in Q'', R''). Average intensity profiles of tiggrin and α-integrin (M'''-N'''), α -integrin and talin (O'''-P'''), and α -integrin and paxillin (Q'''-R''') across the widths of the boxed areas indicated in the corresponding images shown in M''-R''.

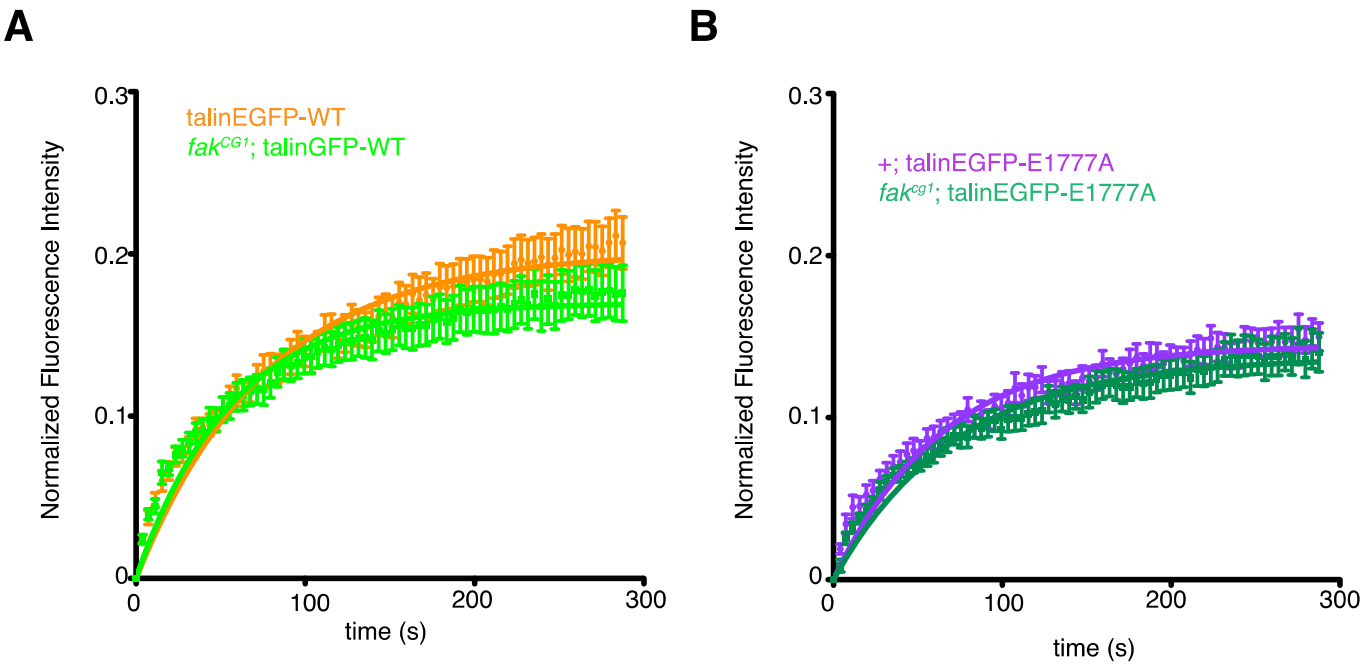

Figure S3. Loss of FAK does not perturb the turnover dynamics of talinGFP or talinGFP*E1777A at MTJs, Related to Figure 3. (A) Fluorescence recovery curve of talinGFP in a WT background and in a FAK null background (*FAK*^{cg1} allele; see [9]). (B) Fluorescence recovery of autoinhibition-impaired talin, talinGFP*E1777A in a WT background and in a FAK null background.

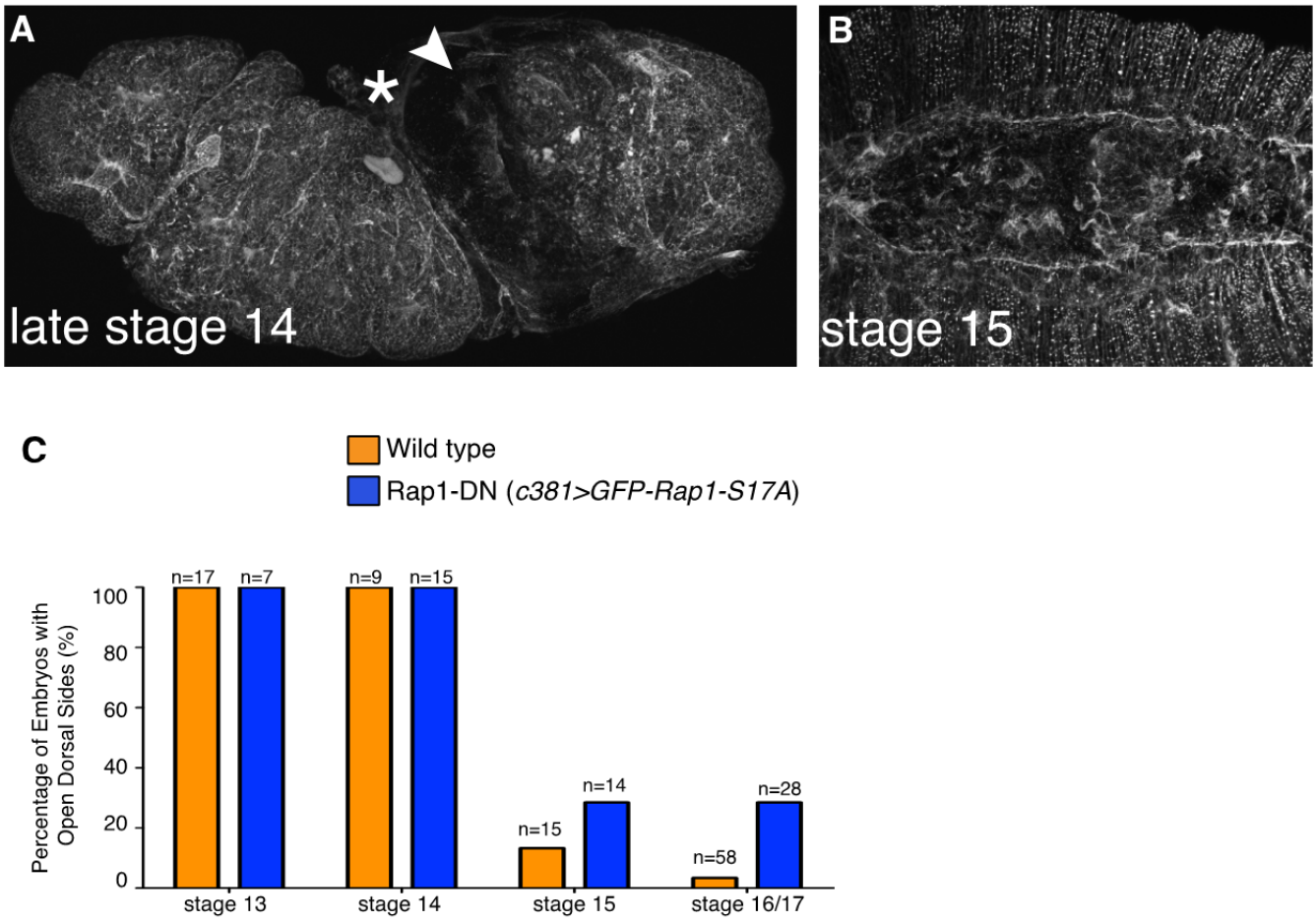

Figure S4. Expression of Rap1-DN in the amnioserosa leads to defects in morphogenesis distinct from the phenotype of expression of Rap1-CA, Related to Figure 3. (A) Stage 14 embryo expressing Rap1-DN in the AS exhibiting both failed dorsal closure (asterisk) and failed germband retraction. (B) Dorsal view of a stage 15 embryo exhibiting a failure to close the dorsal epidermis. (C) WT embryos and embryos expressing Rap1-CA in the AS were scored for openings in the dorsal epidermis at stage 13-17. Rap1-DN expressing embryos exhibited a partially penetrant failure in DC, but a delay in dorsal closure was not observed as a similar proportion of embryos had completed DC at stage 15 as stage 16/17 (Compare to Figs. 1O, 3B, 4B).

Supplemental Experimental Procedures

Molecular Biology and Homology Modeling

The generation of talinGFP is previously described [1]. To make pUbi-talinEGFP*E1777A mutant construct, pBS-talinGFP was mutated using the QuikChange Lightning mutagenesis kit (Stratagene) and the following mutagenesis primers (only forward is shown, change indicated in bold): 5'-cccgttcggtggtgg**c**aagtgccattactct-3'. The talinGFP*E1777A cassette was sub-cloned into the pUbi63E vector using a strategy similar to that used to generate the WT talinGFP construct[1].

To generate Rap1-CA ($Rap1^{Q63E}$) and Rap1-DN ($Rap1^{S17A}$), full-length *Drosophila* $Rap1^{WT}$ cDNA was PCR-cloned into the pCR8/GW/TOPO Gateway Entry Vector (Life Technologies, Grand Island, NY) by TOPO TA cloning. This entry vector served as the template for making $Rap1^{Q63E}$ and $Rap1^{S17A}$ by site-directed mutagenesis (QuikChange, Agilent Technologies, Santa Clara, CA). Rap1 mutant constructs were then recombined into *Drosophila* UASp expression vectors modified for Gateway cloning, using Gateway vectors provided by Terence Murphy (Carnegie Institution for Science, Baltimore, MD). Expression vectors allowed for either a GFP or HA protein fusion at the N-terminus.

mCherry-RIAM30-CAAX (gift of James Lim, CFRI, Vancouver, Canada) was subcloned into a UAST-attB expression vector for fly transgenesis. All transgenic flies were generated by microinjection of fly embryos (BestGene, Chino Hills, CA) with the constructs introduced to the fly genome in a non-site directed way (talin and Rap1 constructs) or by phi31 integrase-mediated transgenesis (RIAM30-CAAX).

The homology-created fly structure of talin helices 37-41 (residues 1655-1826) was created using the program MODELLER[2]. Superposition, RMSD calculations and image rendering in figures 1B, 1C and 1D were performed in PyMol (Schroedinger, Inc.).

Protein expression and purification

Fly talin F2F3 was amplified from talin cDNA and 1662-1828 (R9) was amplified from the *rhea* locus. Each construct was cloned into pLEICS-01 (N-HIS_6 TEV). Constructs were expressed in E. coli BL21 Star (DE3) cultured either in LB, or for preparation of 15N-labeled samples, in minimal media containing 1 g of 15N-ammonium chloride per liter. For the gel filtration and NMR experiments, GST-tagged F2F3 (residues 204-409) talin constructs were purified using glutathione sepharose resin (GE Healthcare) and eluted by TEV cleavage. His-tagged F2F3, R9 (residues 1662-1828) and R9 E1777A were purified on HisTrap HP column (GE Healthcare) and after TEV-cleavage of the tag, by ion exchange. Protein concentrations were determined using extinction coefficients at 280 nm.

Vinculin binding

Analytical gel filtration chromatography using a Superdex-75 (10/300) GL (GE Healthcare) was used to assay binding of the talin R9 domain to the vinculin Vd1 domain. The two domains were incubated together at either 25oC or 42oC for 30 min prior to gel filtration. The column was pre-equilibrated and eluted with 20 mM Tris pH 8.0, 150 mM NaCl and 2mM DTT at a flow rate of 0.8 ml/min at room temperature.

NMR Spectroscopy

Proteins were prepared in 20 mM sodium phosphate pH 6.5, 50 mM NaCl, 2 mM DTT with 10% (v/v) 2H2O. NMR spectra were obtained at 298K using a Bruker AVANCE AVII 800 spectrometer equipped with CryoProbes.

Fly Stocks and Genetics

All rescue experiments were performed in mutant background such that both maternal and zygotic contributions of talin were eliminated, using the *rhea*^{79a} allele and the Dominant Female Sterile technique[3]. Females of the genotype *yw, hs-Flp/+; pUbi-talinGFP*WT or E1777A/+; rhea79a, FRT2A/OvoD1, FRT2A* were subjected to a heatshock-regime during the larval stages to generate mosaic germline in order to give rise to *rhea* mutant oocytes with maternally supplied rescued transgenes. Virgins were then crossed to *rhea*^{79a}*/TM6b, dfd-GMR-nvYFP* males. Embryos without the fluorescent balancer were selected for analyses. For all FRAP experiments, talinGFP constructs were heterozygous and expressed in a *w*^{1118} background. In the case where UAS-driven transgenes were utilized, comparable controls were taken from flies expressing the UAS-transgene, but without the mef2-Gal4 driver. RapCA was driven in the amnioserosa using the c381 driver or the LP1-Gal4 driver (gifts of Nick Harden).

Embryo Staging and Confocal Immunofluorescence Imaging

For all experiments assessing dorsal closure, timed collections were performed to obtain a range of embryos from stage 12-13 (for live imaging), and stages 12-17 for phenotypic quantification of dorsal holes. Since gut morphology was not a consistent or reliable indicator of stage in talin mutants, we used multiple criteria to stage our embryos based on the standard staging markers described in The Atlas of Drosophila Development [4]. The staging criteria used are as follows:

Stage 13 - germband-retraction complete, posterior spiracles apparent

Stage 14 - formation of posterior and anterior canthi

Stage 15 - completion of dorsal closure and re-epithelization, MTJs become prominent, initial formation of epidermal specializations (trichomes), heart-shaped gut

Stage 16 - MTJs fully formed, re-epithelialization of the epidermis at the dorsal midline is complete; multi-constricted gut, onset of muscle contraction

Stage 17 - looped gut, denticle belts formed, mouth hooks visible

Our staging was assisted by the fact that all of our talin-transgene-rescued embryos ubiquitously expressed talinGFP which labels most structures. In the case of embryos that completely failed in DC, the body plan was too disrupted to judge whether embryos were stage 16 or stage 17. For Rap1-CA and Rap1-DN experiments, we performed our phenotypic analysis on fixed embryos stained with rhodamine-conjugated phalloidin to visualize morphology for staging.

Confocal Immunofluorescence Imaging and Image Analysis

Embryos were fixed and stained according to standard protocols. The following antibodies were used in our analysis: rabbit anti-talin (1:500), mouse monoclonal anti-βPS-integrin (1:50; DSHB), rat anti-αPS2-integrin (1:200, 7A10), mouse anti-tiggrin (1:1000; Liselotte Fessler, UCLA), and rabbit anti-paxillin (1:1000; [5]). Rhodamine-conjugated phalloidin (Invitrogen) was used to stain actin filaments (1:400). Fluorescently-conjugated Alexa-Fluor-488, Cy3 and Cy5 secondary antibodies were used at 1:400 dilution (Molecular Probes). Images were collected using an Olympus FV1000 inverted confocal microscope and a UplanFL N 40x 1.30 NA oil objective or a UplanSApo 60x 1.35 NA objective. For all micrographs of whole embryos, or of MTJs, z-stacks were assembled from 8-12 1.0μm confocal sections. For all amnioserosa micrographs, z-stacks were assembled from 3-5 0.6μm confocal sections, just under the apical surface.

For intensity traces across MTJs, the ImageJ plot profile tool was used to determine the average signal intensity across the boxed area indicated on the images. Each channel was independently normalised from unprocessed grey-scale images so that the peak intensity of each channel across the area of interest was set as 100% and the lowest intensity was set to be 0%.

For quantification of βPS-integrin staining in the amnioserosa, all images were taken at identical settings and signal at the cell periphery was quantified according to following formula:

Corrected Fluorescence Intensity = (mean fluorescence of cell periphery)*(area of measured signal) – (mean background fluorescence)*(area of measured signal)

For colocalization analysis of talin and integrin in the amnioserosa, the colocalization feature in Olympus Fluoview software was used to determine Pearson Correlation Coefficients. At least 5 cells in 5 different embryos were used for analysis of β-integrin fluorescence and colocalization in each genotype.

Talin recruitment was quantified as previously described[6, 7] with some modifications as follows: stage 17 embryos were dechorinated in 50% bleach and mounted on a glass slide in PBS. Single confocal images of 1um thickness were collected from 8-10 different confocal planes and the ratio of the MTJ-localized talin to the

cytoplasmically localized talin was measured in each individual plane and then averaged. This was performed for at least 10 different MTJs for each genotype.

Time-Lapse Imaging

For time-lapse movies, stage 13 embryos were dechorinated, glued to a coverslip, dorsal side down, and mounted in Halocarbon Oil 27. Coverslip bridges were used to prevent tissue compression. Using a 40x lens, about 25-30 2.0μm confocal sections were collected at 2-min intervals for an eight-hour time periods using a 473nm laser at room temperature. Several movies were taken of each genotype. Animations were assembled and processed using ImageJ.

FRAP

Stage 17 embryos were collected and prepared for FRAP as described previously [1]. Briefly, embryos were collected from apple juice plates, dechorinated in 50% bleach for 4 minutes, washed with PBS and mounted onto glass slides in PBS. FRAP analysis was performed at room temperature. Photo-bleaching was performed using a 405 nm laser at 30% power with the Tornado scanning tool (Olympus) for 2 seconds at 100 mseconds per pixel. Fluorescence recovery was recorded over 5 minutes at 1 frame every 4 seconds. To control muscle twitching in and out of focus, multiple regions of interest (ROIs) were selected in non-photobleached regions; only samples for which intensities within control ROIs remained steady throughout the FRAP experiment were used. The mobile fraction and statistical tests were performed using Prism 5 software.

qPCR

For the quantitative real-time PCR (qPCR) data shown in supplementary material Fig. S2C, total RNA was isolated from whole flies using TRIzol (Invitrogen) and treated with DNase (Fermentas). A total of 1000 μg total RNA was converted into cDNA using the qScript cDNA Synthesis Kit (Quanta Biosciences). Subsequently, qPCR was performed using the PerfeCTa SYBR Green FastMI ROX kit (Quanta Biosciences). As all talin transgenes were GFP-tagged, we could to quantify transgenic mRNA transcript levels by assaying GFP expression using the primer pair: 5'- GCAGAAGAACGGCATCAAGGT-3' and 5'-ACGAACTCCAGCAGGACCATG-3'. GAPDH mRNA levels were assayed as an internal control using the primer pair: 5'- AAAGCGGCAGTCGTAATAGC-3' and 5'-GACATCGATGAAGGGATCGT-3'. Expression changes were determined by using the comparative Ct method for relative quantitation.

Western Blots

Adult thoraces of wild-type flies expressing TalinGFP and TalinGFP*E1777A mutants were dissected in 50mM Tris, 1mM EDTA, 150mM NaCl, 0.5% Triton, 50% Glycerol and EDTA-free complete protease inhibitor cocktail (Roche) and incubated overnight at -20°C. Samples were homogenized with a mechanical pestle in

50mM Tris, 1mM EDTA, 150mM NaCl, 0.5% Triton and EDTA-free complete protease inhibitor cocktail (Roche) and cleared by centrifugation at 13,000 rpm for 30 min at 4°C. After the addition of SDS sample buffer, samples were heated for 5 minutes at 100°C and separated on a 6% Tris-glycine SDS-polyacrylamide gel before performing a Western Blot. The membrane was blocked in 5% milk for 20 m and incubated with rabbit anti-talin antibody (l:2000, gift of Nick Brown (Gurdon Institute, Cambridge, UK); [8]) or mouse anti-alpha tubulin antibody (1:2000, Sigma) and ECL anti-rabbit or anti-mouse HRP-Conjugated secondary antibody (1:5000, GE) and visualized with ECL Western Blotting Plus Detection system (GE). Quantification of blots was performed using ImageJ (NIH, Bethesda, MD). Westerns were performed in a wild-type background to facilitate comparison of the expression of our GFP-tagged transgenic talin to the untagged endogenous protein. This approach provides important confirmation that the transgenes are sufficiently expressed.

Supplemental References

1. Yuan, L., Fairchild, M.J., Perkins, A.D., and Tanentzapf, G. (2010). Analysis of integrin turnover in fly myotendinous junctions. Journal of cell science *123*, 939-946.
2. Sali, A., and Blundell, T.L. (1993). Comparative protein modelling by satisfaction of spatial restraints. Journal of molecular biology *234*, 779-815.
3. Chou, T.B., and Perrimon, N. (1996). The autosomal FLP-DFS technique for generating germline mosaics in Drosophila melanogaster. Genetics *144*, 1673-1679.
4. Hartenstein, V. (1993). Atlas of Drosophila Development, (Cold Spring Harbor Laboratory Press).
5. Yagi, R., Ishimaru, S., Yano, H., Gaul, U., Hanafusa, H., and Sabe, H. (2001). A novel muscle LIM-only protein is generated from the paxillin gene locus in Drosophila. EMBO reports *2*, 814-820.
6. Tanentzapf, G., Martin-Bermudo, M.D., Hicks, M.S., and Brown, N.H. (2006). Multiple factors contribute to integrin-talin interactions in vivo. Journal of cell science *119*, 1632-1644.
7. Ellis, S.J., Pines, M., Fairchild, M.J., and Tanentzapf, G. (2011). In vivo functional analysis reveals specific roles for the integrin-binding sites of talin. Journal of cell science *124*, 1844-1856.
8. Brown, N.H., Gregory, S.L., Rickoll, W.L., Fessler, L.I., Prout, M., White, R.A., and Fristrom, J.W. (2002). Talin is essential for integrin function in Drosophila. Developmental cell *3*, 569-579.
9. Grabbe, C., Zervas, C.G., Hunter, T., Brown, N.H., and Palmer, R.H. (2004). Focal adhesion kinase is not required for integrin function or viability in Drosophila. Development *131*, 5795-5805.